ION-EXCHANGE SYNTHESIS OF GRAPHENE LOADED-ZnS/Bi$_2$S$_3$ NANOPLATES WITH HIGH PHOTOCATALYTIC ACTIVITY

B. ZENG[a,b*], W. ZENG[a]
**

^aCollege of Mechanical Engineering, Hunan University of Arts and Science, Changde 415000, People's Republic of China
^bHunan Collaborative innovation Center for construction and development of Dongting Lake Ecological Economic Zone, Changde 415000, People's Republic of China

In this work we have prepared graphene loaded-ZnS/Bi$_2$S$_3$ nanoplates. Scanning electron microscopy and transmission electron microscopy observations confirm that two dimensional (2D) ZnS/Bi$_2$S$_3$ nanoplates are tightly anchored on the graphene. The experimental results show that these nanocomposites demonstrate visible-light photocatalytic activities for methyl orange dye degradation. The high visible photocatalytic performances can be attributed to photo-induced electrons-holes separations in the ZnS/Bi$_2$S$_3$ nanoplates and the rapid capture of those electrons by graphene. This work provides a new method for synthesis of these highly efficient visible-light-driven photocatalysts.

1. Introduction

As one of the important II-VI semiconductors, Zinc sulfide (ZnS) appears to be a promising photocatalytic material because of the highly negative redox potentials of its excited electrons and the rapid generation of electron-hole pairs upon photo-excitation [1]. Previous investigations have demonstrated that the morphology, structure, and size of the crystal strongly influence the catalytic activity of ZnS [2]. Two-dimensional nanomaterials have a large specific surface area, providing more reaction sites and direct pathways for electron transport, improving photocatalytic performance [3].

However, because of the wide bandgap for ZnS semiconductors, 3.7-3.8 eV, ZnS absorption is predominantly limited to the UV region [4]. That severely limits the material's practical applications since solar illumination is primary in the visible regime. Many approaches have been taken to resolving this challenge, including combining ZnS with other semiconductors [5], doping it with a metal [6], and loading it with a noble metal [7]. Coupling to a smaller band gap semiconductor has been demonstrated as an effective means of broadening the response to visible light [8]. Bi$_2$S$_3$ has a narrow band gap of 1.3 eV, and has been reported to be an efficient photocatalyst when combined with other semiconductors. For example, Huang et al. prepared novel ZnS/Bi$_2$S$_3$ by simple reflux and cation exchange. The synthesized ZnS/Bi$_2$S$_3$ nanocomposites exhibited a high adsorption capability and photocatalytic activity for methylene blue degradation under UV light irradiation [9]. Gao et al. fabricated a ZnS/Bi$_2$S$_3$ heterojunction with double-layer-tube-shaped structures. Their results showed that Bi$_2$S$_3$ loading significantly improved the photocatalytic activity of ZnS [10]. Wu et al. synthesized ZnS/Bi$_2$S$_3$ heterostructures with an ion-exchange method. Their photocatalysts displayed superior visible light photocatalytic activity [11]. Semiconductor heterojunctions have therefore been demonstrated as potential visible light photocatalysts.

---

*[*]Corresponding author: 21467855@qq.com

Graphene, with a high specific surface area and high electron mobility, is an ideal support for loading nanoparticles [12]. Integrating graphene with different nano-scale materials is therefore an effective way to prevent nanocomposite aggregation. Furthermore, graphene can suppress electron-hole recombination through its conductive network [13]. These properties make graphene integration a promising potential means of enhancing photocatalytic performance. To date however there has been little research into the deposition of 2D ZnS/Bi_2S_3 nanoplates onto graphene.

In this work, we synthesized graphene decorated with ZnS/Bi_2S_3 nanoplates (G-ZnS/Bi_2S_3 NP) using microwave irradiation and ion exchange. Our results reveal that these nanomaterials exhibit high visible-light photocatalytic activities for methyl orange (MO) dye degradation.

2. Experimental details

The G-ZnS nanoplates (G-ZnS NP) were synthesized with the following procedure. 1.83g of zinc acetate $(Zn(AC)_2)$, 0.8g of thioacetamide (TAA), and 0.01g of graphene oxide were blended in octylamine. The blend was microwaved at 300 W for 10 min, producing a brown precipitate. The precipitate was filtered, washed with alcohol in order to remove the reagent (such as $Zn(AC)_2$ and TAA), and centrifuged to obtain the brown powder.

The $G-ZnS/Bi_2S_3$ nanoplates were then synthesized with a simple ion-exchange method using dispersed G-ZnS NP as a precursor. Typically G-ZnS NP are dispersed in 50 mL deionized water and then a certain amount of $Bi(NO_3)_3.5H_2O$ is added to the solution. Ion-exchange was performed for 10 minutes and the precipitate was filtered, washed with distilled water, and dried at 80 ℃ for 12 h. The amount of $Bi(NO_3)_3.5H_2O$ was varied as 1 wt% (sample G-ZnS/Bi_2S_3 NP-1), 5 wt% (sample G-ZnS/Bi_2S_3 NP-5), and 10 wt% (sample G-ZnS/Bi_2S_3 NP-10).

Characterization of the product was carried out with powder x-ray diffraction (XRD, D5000), Raman spectroscopy (J-Y, T6400), fourier transform infrared spectroscopy (FTIR, WQF-410), UV-vis diffuse reflectance spectroscopy (UV-2550), scanning electron microscopy (SEM, S4800), and transmission electron microscopy (TEM, JEM-2100F).

The photocatalytic degradation of MO was measured by degradation of MO aqueous solution (20 mg/L, 300 mL) with 20 mg photocatalyst under the illumination of a 500 W xenon arc lamp. The solution was stirred for 30 min in darkness to reach the adsorption-desorption equilibrium between the photocatalyst and the solution The solution was then irradiated with the xenon arc lamp. Every 3 min a 5 mL aliquot was collected and centrifuged to separate the suspended solid. The absorbance of the supernatant at 464 nm was used to determine the degradation efficiency by UV-vis spectrophotometry.

3. Results and discussion

XRD patterns of the G-ZnS/Bi_2S_3 NP-5 are reproduced in Fig. 1. The diffraction peaks at 26.9°, 28.5°, 31.5°, and 58.1° corresponds to the (100), (002), (101), and (311) planes of ZnS (JCPDS no. 89-2942). The peaks at 40.6°, 63.2°, and 67.3° can be assigned to the (034), (231) and (172) facets of Bi_2S_3. Additionally, an obvious peak at $2\theta = 23°$ can be perfectly assigned as the (002) plane of graphene [14]. No other peaks were detected, indicating high purity.
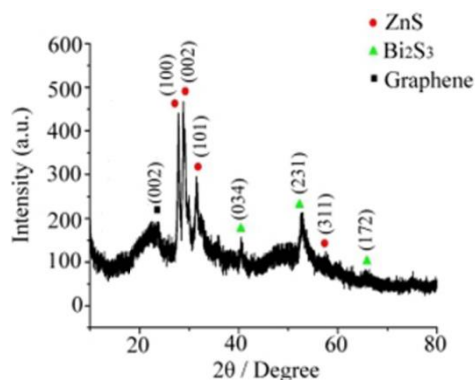
Fig. 1. XRD of G-ZnS/Bi$_2$S$_3$ NP-5 nanocompsites.

Fig. 2 depicts the FTIR spectrum of GO and G-ZnS/Bi$_2$S$_3$ NP-5. For the pure GO, the characteristic peaks at 1074 cm^{-1}, 1375cm^{-1}, 1620 cm^{-1}, 1720 cm^{-1}, and 3403 cm^{-1} were assigned to oxygen-containing functional group oscillations: in that order, alkoxy C-O stretching, carboxyl O-H stretching, H-O-H bending band of the adsorbed H$_2$O molecules, C=O stretching vibrations of carboxyl or carbonyl groups, and H-O stretching vibrations from the surface hydroxyl groups [15]. In the spectrum of G-ZnS/Bi$_2$S$_3$ NP-5, the intensity of these characteristic absorption bands decreased dramatically, indicating an effective reduction of GO by microwave treatment [15]. The absorption band centered at about 500 cm^{-1} was attributed to the metal ion-O stretching vibrations in the nanocomposites, indicating a strong interfacial interaction between graphene and ZnS/Bi$_2$S$_3$ in the composite [16]. All of these findings suggest efficient electron transport, thus enhancing the charge separation and photocatalytic efficiency.
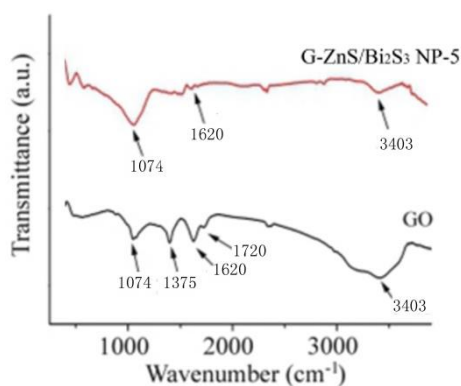

Fig. 2. FTIR spectra of GO and G-ZnS/Bi$_2$S$_3$ NP-5 nanocompsites.

Raman spectroscopy is an effective tool for characterizing the surface microstructure of carbon-based materials. As shown in Fig. 3, GO displayed two prominent Raman response signals, a D band at 1352 cm^{-1} (originating from disruption of the symmetrical hexagonal graphitic lattice by internal structural defects, edge defects, and dangling bonds) and a G band at 1599 cm^{-1} (originating from the in-plane stretching motion of symmetric C−C bonds). The calculated D/G intensity ratio is about 1.08. For G-ZnS/Bi$_2$S$_3$ NP-5, the location of the D and G bands are unaltered while the value of the D/G intensity ratio (I_D/I_G) increases to 1.25, suggesting a decrease in the average size of sp2 domains upon the reduction of GO and the removal of oxygen functional groups in GO [17]. An additional peak observed near 800 cm^{-1} corresponds to surface phonon modes of ZnS/Bi$_2$S$_3$, indicating effective incorporation of ZnS/Bi$_2$S$_3$ into the graphene matrix [17].
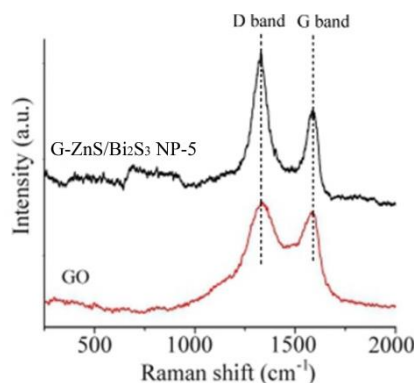
Fig. 3. Raman spectra of GO and G-ZnS/Bi$_2$S$_3$ NP-5 nanocompsites.

The optical absorptivity of the semiconductor is an important factor in determining its photocatalytic performance. As shown in Fig. 4, all of the nanocomposites show strong visible light absorbance because graphene has a wide absorption range. Compared with G-ZnS NP nanocomposites, the system of G-ZnS/Bi$_2$S$_3$ NP nanocomposites show increased absorptivity over the visible range. In the G-ZnS/Bi$_2$S$_3$ NP nanocomposites, the absorption intensity in the visible region becomes stronger with increasing Bi ion concentration, which could be attributed to chemical bonding between ZnS and Bi$_2$S$_3$ [18]. Based on the above results, G-ZnS/Bi$_2$S$_3$ NP composites more efficiently utilize visible light.
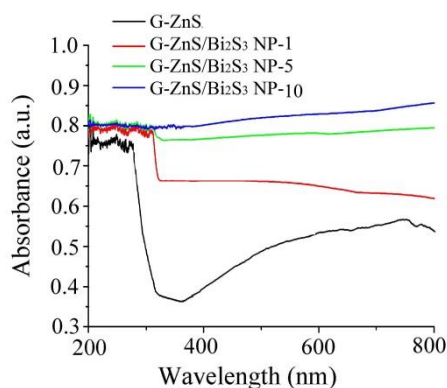

Fig. 4. The UV-vis diffuse reflectance spectra of nanocomposite

Fig. 5 reproduces SEM images of G-ZnS/Bi$_2$S$_3$ NP-5 nanocomposites. It shows that many nanoparticles are densely attached to the surface of graphene. From the close-up SEM image in Fig. 5a we can see that the nanoparticles are circular nanoplates, with a side length of 50-100 nm and a thickness on the order of a few nanometers. The TEM image in Fig. 5b reveals that nanoplates are finely anchored on the surface of graphene. The corresponding HRTEM images of the same G-ZnS/Bi$_2$S$_3$ NP-5 composite in Fig. 5c shows clear lattice fringes. The lattice spaces of 0.31 nm and 0.27 nm could be assigned to the (002) plane of ZnS and the (221) plane of Bi$_2$S$_3$, respectively. To confirm the elemental composition of G-ZnS/Bi$_2$S$_3$-5, EDS was employed (Fig. 5d). The EDS image displays the composite material consisting of zinc, bismuth, sulfur, carbon.
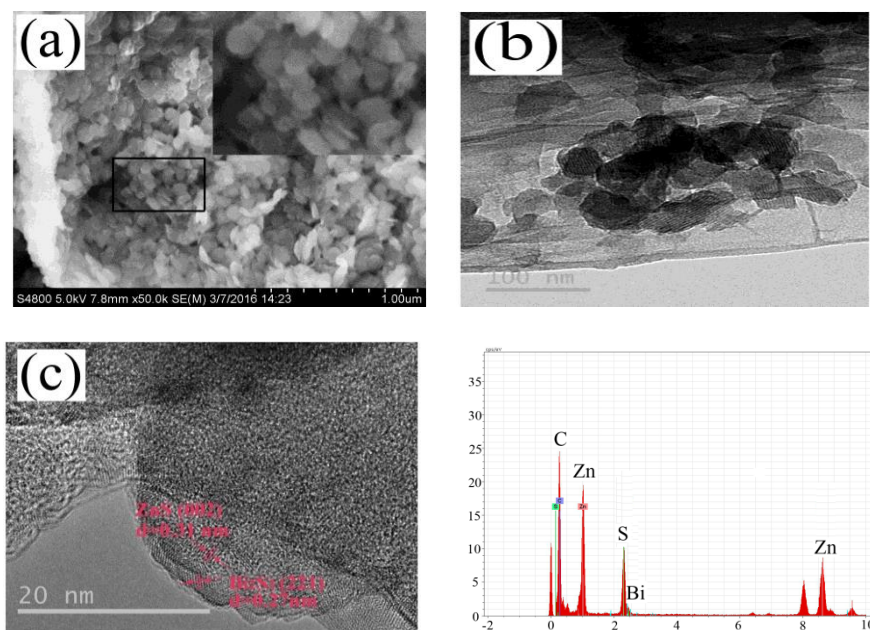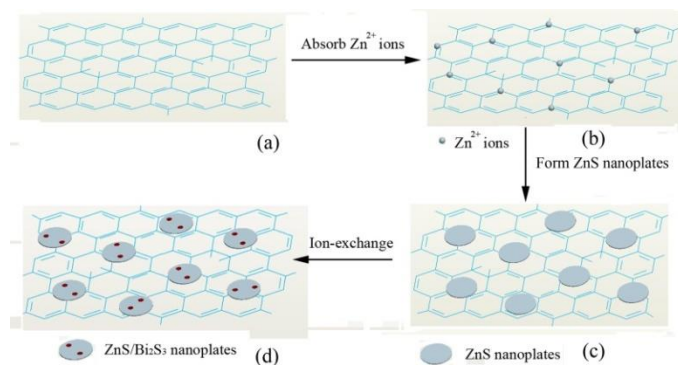
Fig. 5.(a) SEM, (b)TEM. (c)HRTEM, (d)EDX of G-ZnS/Bi$_2$S$_3$ NP-5 nanocomposites

Scheme 1 shows the possible growth process of G-ZnS/Bi$_2$S$_3$ NP. With the addition of Zn(AC)$_2$ and TAA solution into the GO suspension under ultrasonication, the oxygen-containing functional groups on the surface of GO easily anchor Zn^{2+} ions via electrostatic interactions (Scheme 1b) [19]. With the microwave process, circular ZnS nanoplates are formed on the surface of the graphene sheets by a two-dimensional growth mechanism (Scheme 1c) [20]. After the aqueous Bi(NO$_3$)$_2$ is added, the G-ZnS NP readily exchanges Bi^{2+} ions, partially substituting for the Zn in the ZnS nanoplates, thus forming graphene loaded-ZnS/Bi$_2$S$_3$ hetero-nanostructures nanoplates (Scheme 1d) [9-11]. Alongside these steps, graphene oxide is gradually reduced to graphene [21].

Scheme 1. Proposed scheme of the fabricated processes of G-ZnS/Bi$_2$S$_3$ NP.

Fig. 7 shows the photocatalytic activities of different catalysts in the degradation of MO under visible light irradiation. No photolysis of MO is observed when no catalyst or only graphene are added. When G-ZnS NP is added, substantial degradation (47.1%) of MO is observed in 180 min under visible light. The introduction of Bi$_2$S$_3$ reduces the degradtation to 30.2%, 18.2%, and 22.1% for the 1, 5, and 10 wt% samples, respectively. ZnS/Bi$_2$S$_3$ NP therefore provide a clear advantage in the G-ZnS/Bi$_2$S$_3$ NP system. G-ZnS/Bi$_2$S$_3$ NP-5 displays the best photocatalytic MO degradation efficiency, suggesting that the content of Bi$_2$S$_3$ significantly affects the photocatalytic activities of G-ZnS/Bi$_2$S$_3$ NP.
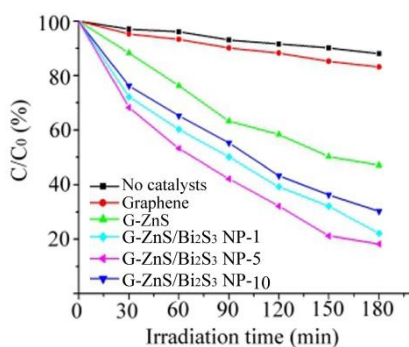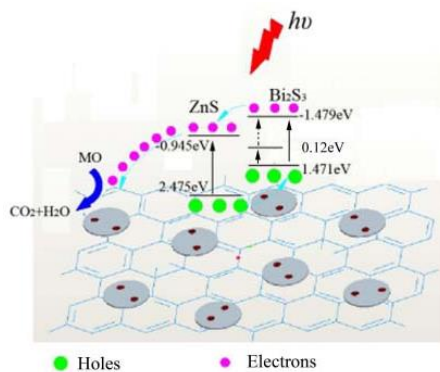
Fig. 7. Photocatalytic degradation efficiency of MO with different catalysts under visible light.

Based on the above results, possible charge separation processes are proposed in Scheme 2. With a narrow band gap energy (1.39 eV) Bi_2S_3 could be excited by visible light (λ >420 nm) and induce the generation of electron-hole pairs. Those pairs however easily recombine [11]. ZnS cannot be excited by visible light due to its wide energy gap of 3.42 eV [11]. When the ZnS/Bi_2S_3 composite is synthesized, electrons in the valence band of Bi_2S_3 can be excited and transfer to a higher potential edge for higher photon energy [11]. Then electrons in the CB of Bi_2S_3 (−1.479 eV) could easily transfer to the CB of ZnS (−0.945 eV) driven by the difference in potentials, leaving holes in the Bi_2S_3 valence band. Thus the photo-generated electron-hole pairs are separated effectively [11]. As an effective electron collector and transporter, graphene can capture the photo-generated electrons in the CB of ZnS. Consequently, the photo-induced electrons (both on the surface of the graphene and on the surface of the semiconductor) could instigate radical formation, greatly enlarging the reaction space [22]. However, with excess Bi_2S_3 in the composite, photoinduced electrons and holes would recombine easily, consequently reducing the photocatalytic activity of the ZnS/Bi_2S_3 composite photocatalyst.

Scheme 2. Schematic illustration for the charge transfer and separation in the G-ZnS/Bi$_2$S$_3$ NP system.

4. Conclusions

Graphene-loaded 2D ZnS/Bi_2S_3 nanoplates are prepared via microwave irradiation and ion exchange. These nanostructures show highly efficient visible-light-driven photocatalytic activities for dye degradation. When the ZnS/Bi_2S_3 nanoplates forms heteronanostructures on the graphene, an obvious visible-light response can be observed. The enhanced activities of G-ZnS/Bi$_2$S$_3$ nanoplates heteronanostructures can be attributed to the effective separation of photoinduced carriers in the ZnS/Bi_2S_3 nanoplates and the rapid capture of those electrons by graphene. This work provides helpful insight in the design of highly efficient visible-light-driven photocatalysts.

Acknowledgment

References

[1] H.L Zhang, B. Wei, L. Zhu, et al. Appl. Surf. Sci. **270**, 133 (2003).
[2] J.F. Lu,X.H. Zeng, H.F. Liu, et al. Mater. Lett. **93**, 337 (2013).
[3] X.J. Bian, X.F. Lu, Y.P. Xue, et al. J Colloid Interf. Sci.**406**, 37 (2013).
[4] X.D. Zhang, X.J. Liu, L. Zhang, et al. J Alloys Compd. **655**, 38 (2016).
[5] D.A. Reddy, R. Ma, M.Y. Choi, et al. Appl. Surf. Sci. **324**, 725 (2015).
[6] X.J. Wang, Q.L. Zhang, B.S. Zou, et al. Appl. Surf. Sci. **257**, 10898 (2011).
[7] J.Y. Zhang, Y.H. Wang, J. Zhang, et al. ACS Appl. Mater. Interf. **5**(3), 1031 (2013).
[8] J. Zhang, J.G. Yu, Y.M. Zhang, et al. Nano lett. **11**, 4474 (2011).
[9] D.N. Xiong, G.F. Huang, B.X. Zhou, et al. J Colloid Interf. Sci. **464,** 103 (2016).
[10]X.M. Gao, Z.H. Wang, F. Fu, et al. Physica B **474**, 81 (2015).
[11] Z.D. Wu, L.L. Chen, C.S. Xing, et al. Dalton T. **42**, 12980 (2013) -12988.
[12] Q. Xiang, J. Yu, M. Jaroniec. Chem. Soc. Rev. **41**, 782 (2012).
[13] N. Zhang, Y. Zhang, Y.-J. Xu. Nanoscale **4**, 5792 (2012).
[14] Q. Li, B. Guo, J. Yu, et al. J Am. Chem. Soc. **133**, 10878 (2011).
[15] M. Shah, A. Park, et al. ACS Appl. Mater. Interf. **4**, 3893 (2012).
[16] L.J. Gu, J.Y. Wang, H. Cheng, et al. ACS Appl. Mater. Interf. **5**, 3085 (2013).
[17] V.A. Naveenb, V.P. Kamalakannana, et al. Appl. Surf. Sci. **351**, 635 (2015).
[18] X.G. Li,Y.L. Li, J.F. Shen, et al.. Ceram. Int. **42**, 3154 (2016).
[19] J. Zhu, Y. Li, Y. Chen, et al.. Carbon **49**, 1900 (2011).
[20] H. Hu, X. Wang, F. Liu, et al. Synth. Metal **161**, 404 (2011).
[21] B. Zeng, X.H. Chen. J Alloys Comp. **582,** 774 (2014).
[22] B. Zeng, X.H. Chen, Y.X. Luo, et al. Ceram. Inter. **40**, 5055 (2014).